ACS APPLIED MATERIALS & INTERFACES

Research Article

www.acsami.org

Single-Walled Aluminosilicate Nanotube/Poly(vinyl alcohol) Nanocomposite Membranes

Dun-Yen Kang,[†] Ho Ming Tong,[†] Ji Zang,[†] Rudra Prosad Choudhury,[‡] David S. Sholl,[†] Haskell W. Beckham,[‡] Christopher W. Jones,*[,†] and Sankar Nair*[,†]

[†]School of Chemical & Biomolecular Engineering, and [‡]School of Materials Science and Engineering, Georgia Institute of Technology, Atlanta, Georgia 30332, United States

Supporting Information

ABSTRACT: The fabrication, detailed characterization, and molecular transport properties of nanocomposite membranes containing high fractions (up to 40 vol %) of individually-dispersed aluminosilicate single-walled nanotubes (SWNTs) in poly(vinyl alcohol) (PVA), are reported. The microstructure, SWNT dispersion, SWNT dimensions, and intertubular distances within the composite membranes are characterized by scanning and transmission electron microscopy (SEM and TEM), energy-dispersive spectroscopy (EDS), X-ray diffraction (XRD), XRD rocking curve analysis, small-angle X-ray scattering (SAXS), and solid-state NMR. PVA/SWNT nanocomposite membranes prepared from SWNT gels allow uniform dispersion of individual SWNTs in the PVA matrix with a random distribution of orientations. SAXS analysis reveals the length (~500 nm) and outer diameter (~2.2 nm) of the dispersed SWNTs. Electron microscopy indicates good adhesion between the SWNTs and the PVA matrix without the occurrence of defects such as voids and pinholes. The transport properties of the PVA/SWNT membranes are investigated experimentally by ethanol/water mixture pervaporation measurements, computationally by grand canonical Monte Carlo and molecular dynamics, and by a macroscopic transport model for anisotropic permeation through nanotube−polymer composite membranes. The nanocomposite membranes substantially enhance the water throughput with increasing SWNT volume fraction, which leads to a moderate reduction of the water/ethanol selectivity. The model is parameterized purely from molecular simulation data with no fitted parameters, and shows reasonably good agreement with the experimental water permeability data.

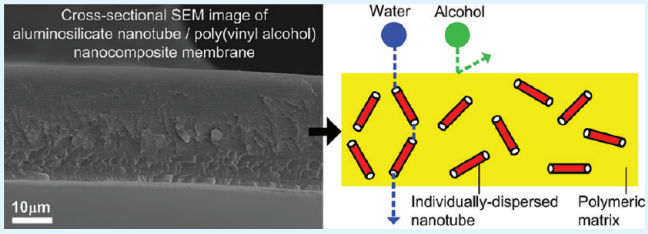

KEYWORDS: *nanotube, membrane, metal oxide, nanocomposite, separation*

INTRODUCTION

The synthesis, properties, and applications of nanotube materials have been extensively studied for more than two decades.[1−5] Carbon nanotubes have been found to possess good mechanical,[6,7] electrical,[8] thermal,[9,10] and mass transport[11,12] properties and can be incorporated into other solid-phase materials as nanoscale fillers. The mechanical and electrical/heat/mass transport properties of such nanocomposites exhibit a strong dependence on the filler volume fraction.[10,13,14] Previous studies have also suggested that uniformity of the nanotube dispersion in the matrix material plays a critical role in the performance enhancement. For example, carbon nanotube/polymer composite membranes with non-ideal nanotube dispersion (i.e., aggregation of nanotubes in the matrix due to the incompatibility between the outer surface of the carbon nanotubes and the matrix materials) were found to yield low molecular selectivity.[2,15] Furthermore, nanotube dispersion and defect regions in carbon nanotube-based composite membranes have not yet been fully characterized. As a result, the relative contributions to mass transport from the dispersed nanotubes (pore size <10 nm) and the defect regions (of size ~1 μm) are unclear.[16,17] To address the problem of increasing the nanotube loading in nanocomposites while maintaining good dispersion, a range of techniques for outer surface modification of carbon nanotubes have been developed, such as the use of surfactants[18−22] or *in situ* polymerization[22−26] to enhance the nanotube compatibility with the polymeric matrix. Nevertheless, the highest volume fraction reported to date of carbon nanotubes dispersed in a polymeric material without significant nanotube aggregation is only about 20 %.[10,27] This limitation hinders the performance enhancement that the nanotubes can potentially create in a composite material or membrane.

The limits on carbon nanotube loading in composite materials are likely related to the difficulty of dispersing the nanotubes individually in a liquid prior to preparing the solid-phase composite.[28−31] However, individual dispersion of nanotubes in polar liquids can be achieved in the case of metal oxide nanotubes that are synthesized hydrothermally or solvothermally and have polar surfaces.[32−37] Single-walled aluminosilicate nanotubes (SWNTs, Figure 1), which are synthetic analogues of the nanotubular mineral imogolite, can

Received: November 18, 2011
Accepted: January 19, 2012
Published: January 19, 2012

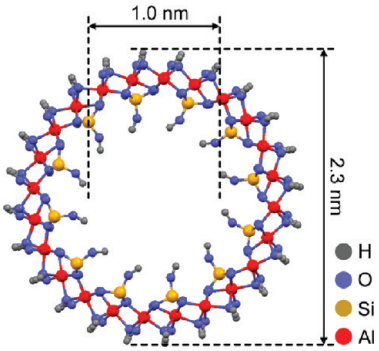

Figure 1. Structure of the aluminosilicate single-walled nanotube.

be synthesized hydrothermally with a high degree of dispersion.[35,38−40] These SWNTs are hypothesized to be amenable to the fabrication and application of high-loading nanotube composites with near-ideal dispersion of nanotubes. Furthermore, previous studies have suggested that aluminosilicate SWNTs possess extraordinarily high interior hydrophilicity due to their high inner surface silanol densities,[41,42] and membranes incorporating them have been predicted to exhibit excellent water transport properties and good water/alcohol selectivity.[43−45] The transport properties of these materials can also be controlled by internal surface modification[46,47] and tuning of the nanotube diameter.[48,49] Therefore, SWNT/polymer composite membranes are interesting candidates for applications in water/organic separations (e.g., water/ethanol separation as encountered in biofuel production).

In this work, we report the preparation, characterization, and permeation properties of polymer/SWNT composite membranes with high loading and near-ideal dispersion of nanotubes. Specifically, the loading of well-dispersed SWNTs in poly(vinyl alcohol) (PVA) membranes is systematically increased up to 38% by volume. The importance of initial dispersion of the SWNTs in a liquid medium is highlighted by comparison of membranes fabricated using SWNT gels and SWNT powders as starting materials. The microstructure of the composite membranes is assessed qualitatively and quantitatively by scanning electron microscopy (SEM), energy-dispersive spectroscopy (EDS), 2D X-ray diffraction (XRD), small-angle X-ray scattering (SAXS) and solid-state NMR. Subsequently, the permeation properties of the PVA/SWNT composite membranes are studied by water/ethanol pervaporation measurements, and the results are analyzed in terms of recently-developed models for transport in polymer/nanotube composite membranes as well as with predictions from molecular simulation studies.

EXPERIMENTAL SECTION

Preparation of Aluminosilicate SWNTs. Tetraethyl orthosilicate (TEOS) was mixed with aluminum-tri-*sec*-butoxide in a glove box filled with nitrogen. The mixture was added to an aqueous 75 mM perchloric acid solution with a molar ratio Si:Al:$HClO_4$ = 1.1:2:1, under vigorous stirring at room temperature in ambient conditions for 24 h. The solution was then diluted with DI water by a factor of 3.8 and was stirred at 95°C for 4 days. Once the temperature was brought to 95°C, the solution turned from cloudy to clear in about one hour. After the solution was cooled to room temperature, a 30 wt % ammonia solution was added dropwise until gelation of the suspended nanotubes occurred. The gel was isolated by centrifugation at 7000 rpm for 10 min. The supernatant was discarded and a few drops of 10 N hydrochloric acid were added to the gel, thereby redispersing the nanotubes. The resulting gel was purified by dialysis against DI water for 3 days using a membrane with a molecular weight cutoff of 15 kDa. Part of the purified suspension was used to prepare PVA/SWNT-gel composite membranes, and the remaining part was dried at 60 °C and then ground lightly to obtain a powder sample of the SWNTs for preparing PVA/SWNT-powder membranes. Approximately one gram of SWNT powder sample is obtained by a 1 L synthesis batch.

Preparation of Aluminosilicate SWNT/PVA Composite Membranes with SWNT Powders. The SWNT powder sample was weighed and mixed with 30 mL of PVA aqueous solution at room temperature. The total mass of SWNT and PVA was 400 mg and the mass fractions of SWNT were controlled at 0.1, 0.2, 0.3, and 0.4, respectively. The resulting PVA/SWNT mixture was gently stirred for 18 h at room temperature. The mixture was then poured into a polystyrene petri dish and the membrane was cast at 60 °C for 24 h. The resulting composite membrane was removed from the petri dish and placed in a crosslinking bath containing 50 mL of water, 50 mL of acetone, 0.5 g of 98 wt % sulfuric acid, and 1.25 g of 25 wt % glutaraldehyde for 30 min. The crosslinked membrane was washed with ethanol and then dried at 60 °C for 24 h. The SWNT volume fractions of the resulting membranes were determined from the mass fractions and densities of SWNTs and PVA. Details of the calculation of SWNT volume fractions are shown in the Supporting Information. Membranes with SWNT volume fractions of 0.11, 0.21, 0.31, and 0.42 are referred to as pwd-1, pwd-2, pwd-3, pwd-4, respectively, in the following discussion. These membranes have thicknesses in the range of 40−100 μm, as determined by a screw gauge as well as cross-sectional SEM images.

Preparation of Aluminosilicate SWNT/PVA Composite Membranes with SWNT Gel. SWNT gels (8, 16, 24, and 32 mL) were mixed at room temperature with 20 mL of PVA aqueous solutions containing 360, 320, 280, and 240 mg of PVA, respectively. The PVA/SWNT composite membranes were then cast and crosslinked by the same procedures mentioned in the previous section. The SWNT mass fractions in the resulting PVA/SWNT membranes were determined by thermogravimetric analysis (see the Supporting Information). The SWNT volume fractions were determined as mentioned in the previous section. Membranes with SWNT volume fractions of 0.08, 0.20, 0.33, and 0.38 are referred as gel-1, gel-2, gel-3, and gel-4, respectively, in the following discussion. These membranes have thicknesses in the range of 40-100 μm, as determined by a screw gauge as well as cross-sectional SEM images.

Electron Microscopy and Energy-Dispersive Spectroscopy (EDS). The morphology of SWNT/PVA composite membranes was imaged with a scanning electron microscope (SEM, Hitachi S-3700N). To observe the cross-sectional morphology, we cryogenically fractured the membranes in liquid N_2. Energy-dispersive spectroscopy (EDS) analysis of the cross-sections was carried out with the same instrument. Transmission electron microscopy (TEM) was used to image SWNTs dispersed in the polymeric matrix. The membrane was embedded in epoxy and then microtomed into approximately 100 nm slices, which were collected on 300 mesh copper grids coated with Formvar layers. TEM images were recorded on a Hitachi HF2000 field-emission TEM at 200 kV.

XRD Measurements and Simulations. X-ray diffraction (XRD) scans in Bragg-Brentano geometry were performed on a PAnalytical X'pert Pro MPD diffractometer operating with a Cu Kα source. Diffraction data were collected with a collimator and Miniprop detector, in the range of 3−30° 2θ and a step size of 0.05°. Grazing-angle XRD scans were performed on PAnalytical X'pert Pro MRD diffractometer operating with a Cu Kα source. The diffraction patterns were recorded with a collimator and Miniprop detector scanning from 0−90° ϕ and a step size of 0.05°, at fixed 2θ values of 4.6 and 19.5° in order to probe the orientation of SWNTs and PVA polymer chains, respectively. XRD simulations were performed to investigate the extent of SWNT bundling. The Reflex module of the Materials Studio 3.2 molecular simulation package (Accelrys, Inc.) was used, and the details of such simulations have been reported in our previous works.[41]

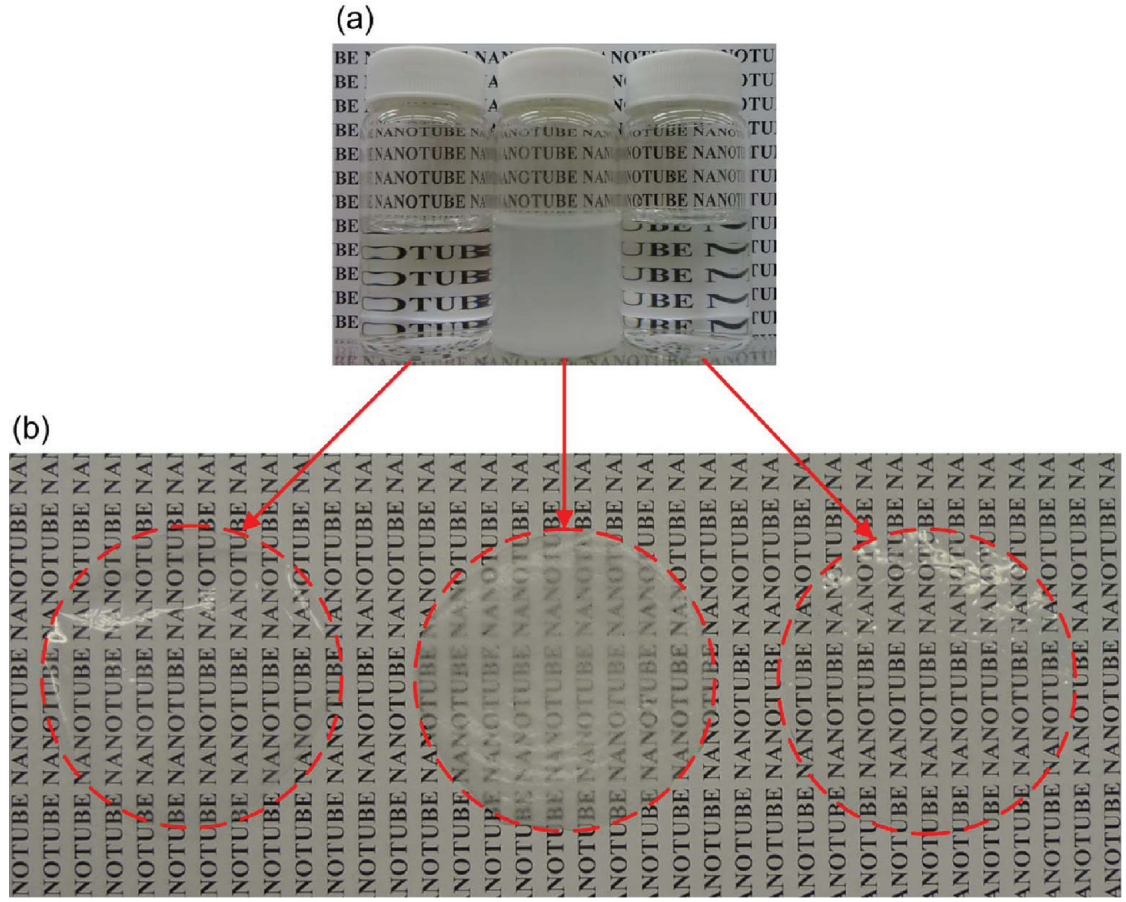

Figure 2. Photographs of (a) aqueous solutions (or dispersions) of pure PVA, SWNT powder, and SWNT gel from left to right; (b) a pure PVA membrane, a powder-derived ~40 vol % SWNT/PVA membrane, and a gel-derived ~40 vol % SWNT/PVA membrane, from left to right. The red circles locate the membranes of 3″ diameter.

SAXS Measurements and Simulations. Small-angle X-ray scattering (SAXS) on the prepared membranes were performed on the DND-CAT beamline at the Advanced Photon Source (Argonne National Laboratory). The beamline was tuned to operate at 17 keV , resulting in an X-ray wavelength of 0.73 Å. The beam at the sample position was controlled to have dimensions of a few hundred micrometers. The SAXS patterns of SWNT/PVA composite membranes were simulated as described in the Results and Discussion section, and key structural parameters were obtained by fitting the model predictions to the measured data.

Pervaporation. The composite membranes were used for pervaporation of an ethanol/water mixture. The feed solution was 80 wt % ethanol. The measurements were performed at 60 °C, wth a feed and permeate pressure of 101 kPa and 0.5 kPa, respectively. Two cold traps at 77 K were used to collect the permeate. After 2 h of permeation, the cold traps were weighed in order to obtain the total permeate mass flow rate. The total mass flux was determined by dividing the mass flow rate by the membrane area (18.8 cm^2). The permeate composition was measured by a gas chromatograph (GC). The water and ethanol molar fluxes (J) thus obtained were converted into water and ethanol permeability by the relation $J = P_{eff}(\Delta p/t)$, where P_{eff} is the effective permeability of the membrane for the transported molecules, t is the thickness of the membrane, and Δp is the vapor pressure difference of the transported molecules between the feed side and the permeate side.[50] The membrane thicknesses were measured by a spring thickness gauge. In order to obtain Δp, the vapor pressures of water and ethanol on the feed side and on the permeate side were determined separately. The water or ethanol vapor pressures on the feed side were taken as the product of its liquid phase mole fraction, its saturated vapor pressure, and its activity coefficient for the mixture. The liquid phase mole fraction was measured by GC. The saturated vapor pressures and the activity coefficient were estimated by the Antoine equation[51] and the UNIFAC model[51] respectively. The water or ethanol vapor pressures on the permeate side were the product of the measured pressure on the permeate side and its mole fraction on the permeate side measured by GC.

Molecular Adsorption and Diffusion Simulations. The construction and the structural optimization of SWNT atomic models is described in our previous works.[43−45,48] Adsorption isotherms were calculated at 333 K for single-component water and ethanol using the Grand Canonical Monte Carlo (GCMC) method as implemented in the MUSIC simulation code,[52] with the molecules only allowed to be inserted within the NT pore. The CLAYFF[53] force field for NTs, the SPC model for water, and the TraPPE[54] force field for ethanol were used as explained in our previous work.[44,48,55,56] The flexibility of hydroxyl groups was considered as described previously,[55] with all atoms in the NTs being fixed in position except for the surface hydroxyl groups. To examine the diffusion of water and ethanol in NTs, we performed NVT molecular dynamics (MD) simulations at 333 K using a Nosé-Hoover thermostat. Unlike our GCMC calculations, all atoms in the NTs were allowed to move in the MD calculations. After equilibrating the system for 0.4 ns, MD simulations were run for 2 ns with a time step of 1 fs. The corrected diffusivities (D_0),[57] which describe the diffusive motion of the center-of-mass of the molecules relative to the reference frame of the adsorbent, were calculated by averaging data over 30 independent trajectories for water and ethanol loadings ranging from near-zero to near-saturation loading. Transport diffusivities (D_t),[57] which describe the macroscopic diffusive transport under the influence of a concentration gradient, were then calculated from D_0 and the thermodynamic correction factor: $D_t = D_0 \partial \ln f/\partial \ln C$. Here, f is the fugacity of the bulk gas phase in equilibrium with the concentration C of the species in the adsorbed

dx.doi.org/10.1021/am201614w | ACS Appl. Mater. Interfaces 2012, 4, 965−976

phase. The thermodynamic correction factor $\partial \ln f/\partial \ln C$ was obtained from the computed adsorption isotherms by assuming fugacity and pressure to be equal in the pressure range considered in this study. The permeability (P) at a given pressure (p) is taken as $P = D_t(C)C/p$, where C is the concentration of species in the adsorbed phase at the given pressure. The permeability information for the pressure range of the pervaporation experiments (p = 101 kPa for the feed side and p = 0.5 kPa for the permeate side) was thus obtained.

Solid-State NMR. ^{1}H and ^{1}H→^{13}C cross-polarization (CP) solid-state NMR measurements were performed on a Bruker DSX 400 spectrometer operating at resonance frequencies of 399.8 MHz for ^{1}H and 100.5 MHz for ^{13}C. The membranes were cut into small pieces and packed tightly into a 4 mm rotor. The rotor was spun at frequency of 10 kHz during the measurements. A $\pi/2$ pulse and 4 s repetition time were applied for both ^{1}H and ^{13}C measurements. Chemical shifts of the ^{1}H and ^{13}C spectra were referenced to adamantane.

RESULTS AND DISCUSSION

Uniformity of PVA/SWNT Composite Membranes. Photographs of the aqueous PVA/SWNT solutions and PVA/SWNT membranes prepared by the two different starting materials (SWNT gels and SWNT powders) are summarized in Figure 2. The pure PVA solution, and the solution used for preparing the gel-4 membrane, both show high transparency in comparison to the PVA/SWNT solution used for preparing the pwd-4 membrane (Figure 2a). This suggests that any aggregates/bundles of nanotubes in the sample are smaller than the smallest wavelength of visible light (~390 nm). On the other hand, suspended particles can be visually observed in the pwd-4 solution, which implies that the SWNT particles do not completely redisperse into individual SWNTS in a pure aqueous solution with no pH adjustment. As seen from Figure 2b, the membrane made from the gel-4 solution shows transparency similar to pure PVA membranes, thereby indicating no severe phase separation during membrane formation and good dispersion of the SWNTs in the solid phase. In contrast, the low transparency of the pwd-4 membrane implies the aggregation of SWNT particles in the membrane.

Figure 3 shows cross-sectional SEM images and EDS line profiles of the silicon-to-carbon intensity ratio for membranes prepared from SWNT powder (pwd-4) and SWNT gel (gel-4). Similar results are obtained for the remaining membranes in our sample set, and are shown in the Supporting Information. The pwd-4 membrane (Figure 3a) displays the existence of large SWNT agglomerations that have a high silicon-to-carbon intensity ratio in EDS. (SEM images and EDS line profiles of samples pwd-1, pwd-2, and pwd-3 are presented in the Supporting Figure S3, and SEM images of the SWNT powder sample are shown in the Supporting Information, Figure S4). However, although the SWNT aggregates do not completely dissociate during membrane formation, the absence of micrometer-scale voids between the SWNTs and the PVA matrix suggests good adhesion properties between the two materials. This is likely due to the interaction of the hydroxyl groups of PVA with the bridging hydroxyl groups on the outer surface of the SWNTs. Membranes prepared with SWNT gels exhibit a homogeneous appearance in the cross-sectional SEM image and the EDS profile (Figure 3b–e), thereby suggesting that the SWNTs are uniformly dispersed. Additionally, a monotonic increase of the silicon-to-carbon ratio is observed in the SWNT gel membranes upon increasing the SWNT volume fraction (Figure 3b and the Supporting Information, Table S3). Visual evidence of SWNTs in the SWNT gel membranes is also

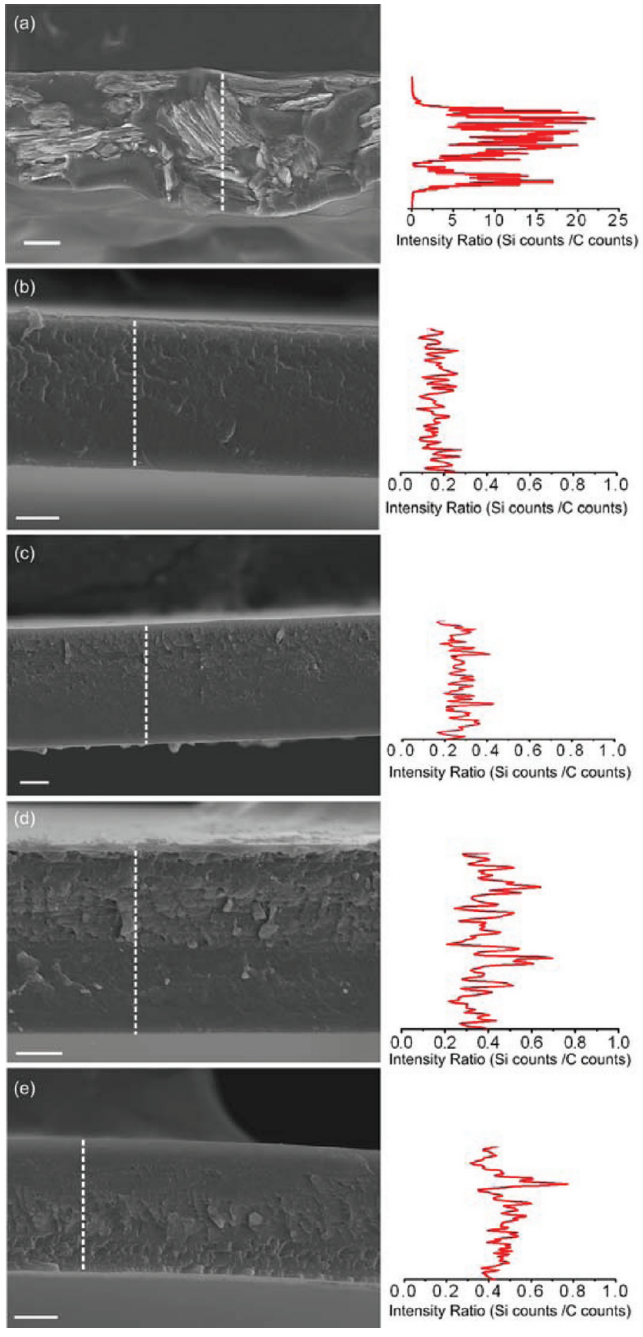

Figure 3. SEM images (left) and line profiles of silicon/carbon intensity from EDS patterns (right) for PVA/SWNT membranes prepared by SWNT powders or gels: (a) pwd-4, (b) gel-1, (c) gel-2, (d) gel-3, and (d) gel-4. The vertical dashed lines represent the locations where EDS line profiles were measured. The scale bars represent 10 μm.

obtained from cross-sectional TEM images (see the Supporting Information, Figure S5). The mean and standard deviation of the silicon-to-carbon ratio are summarized in the Supporting Information, Table S1, with a spatial resolution of 0.1 μm. The membranes prepared using SWNT gels yield much more uniform SWNT dispersion than those prepared by SWNT powders.

Bundling and Orientation of SWNTs in Composite Membranes. Solid-state X-ray diffraction and scattering are excellent probes of SWNT bundling, orientation, dimensions

and dispersion in a solid medium. X-ray diffraction (XRD) with respect to the Bragg angle 2θ can be used for assessing the bundling of SWNTs, grazing angle X-ray diffraction with respect to the azimuthal angle ϕ can be used to investigate the SWNT orientation, and small-angle X-ray scattering (SAXS) can quantitatively elucidate the dimensions and dispersion of SWNTs in the composite membranes. The diffraction patterns of nanotubes forming small bundles are not dominated by Bragg diffraction but by X-ray scattering. In contrast to ordered porous materials such as one-dimensional zeolites, MCM-41, or SBA-15, the small bundles (e.g., bundles with fewer than 25 individual nanotubes) in nanotube materials do not provide sufficient long-range periodicity for Bragg diffraction.[41,58,59] Hence, an explicit atomic-scale simulation of X-ray scattering from a finite-size bundle is a more reliable tool for predicting the XRD patterns. Such simulations have been previously carried out for the aluminosilicate SWNTS and have elucidated their bundling characteristics in powder form.[41] Figure 4a summarizes experimental XRD patterns from SWNT powder samples and simulated patterns from different bundling arrangements. The simulated patterns clearly indicate a shoulder at 5−6° 2θ as being the main difference between isolated SWNTs and bundled SWNTs. Considering the presence of this peak at 5−6° 2θ in the XRD pattern of as-synthesized SWNT powder sample, it has been concluded that the SWNTs in the powder samples are not individually dispersed but instead form small 2 × 2 or triangular bundles.[41] Simulated XRD patterns of SWNTs with various bundling arrangements (3 × 3, 4 × 4, etc.) were also reported in our previous work.[41]

The XRD patterns of PVA/SWNT membranes prepared from powder samples (Figure 4b) show clear shoulder peaks for pwd-2, pwd-3, and pwd-4, indicating that the SWNT powders do not fully redisperse into individual SWNTs in the composite membranes. This observation is consistent with the SEM images, where SWNT agglomerated particles are observed in the PVA matrix. The shoulder peak in the pwd-1 sample is more difficult to observe due to the low signal-to-noise ratio of the nanotube scattering intensity at low volume fractions. The sharp peak at 19.5° 2θ in all the membrane samples is due to the crystallinity of PVA polymer chains,[60] and is also observed in pure PVA membranes (see the Supporting Information). Composite membranes prepared using SWNT gel samples (gel-1, gel-2, and gel-3) show the absence of the shoulder peak at 5−6° 2θ (Figure 4c), and these experimental patterns match the simulated pattern of an isolated SWNT (Figure 4a), providing clear evidence that the SWNTs disperse in the PVA matrix as isolated SWNTs. The PVA chains may effectively penetrate the loosely coordinated network of SWNT-water bonds existing in the gel, but are not likely able to penetrate the interstices between SWNTs in the powder. In other words, the methodology of preparing PVA/SWNT composites starting from SWNT gels overcomes the problem of obtaining individually dispersed SWNTs in a polymer matrix with high loadings (> 20 vol %).[10,27] An XRD "rocking curve" analysis for assessing the degree of orientation of SWNTs in the PVA matrix is presented in the Supporting Information. These results suggest that the SWNTs are almost randomly oriented in the membranes prepared from SWNT gels as well as powders.

Small-angle X-ray scattering (SAXS) can be used to assess the intertubular distances between SWNTs in the polymeric matrix. For well-dispersed cylindrical particles, the trans-

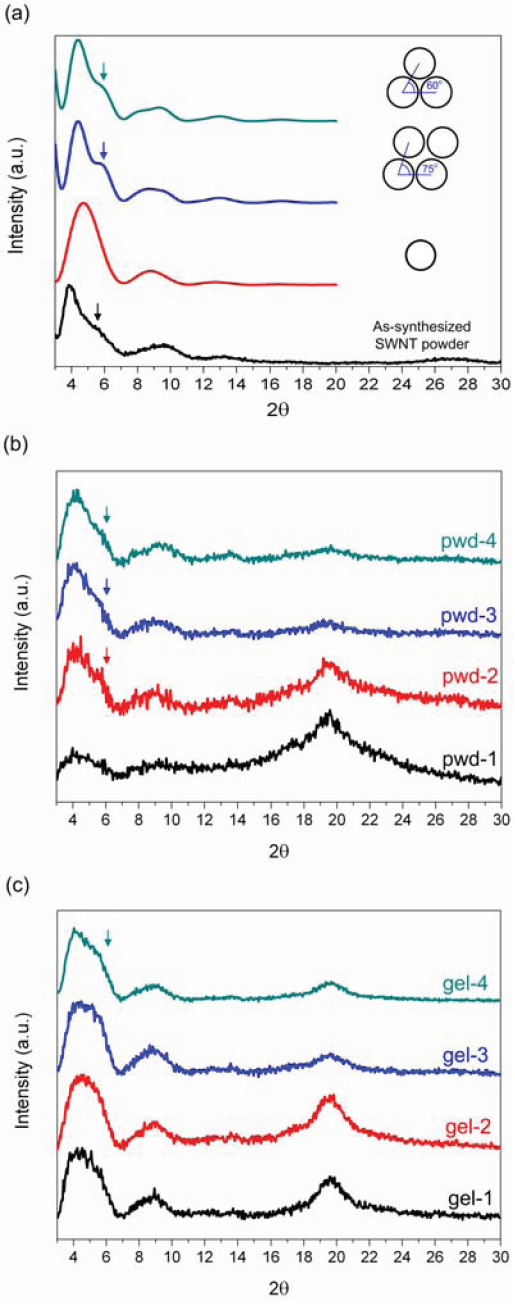

Figure 4. (a) Experimental SWNT XRD pattern (bottom), and simulated XRD patterns of isolated SWNTs and SWNT bundles with different bundling arrangements. The arrows indicate the shoulder peak distinctive to bundle formation. (b) XRD patterns for PVA/SWNT membranes prepared from SWNT powders. (c) XRD patterns for PVA/SWNT membranes prepared from SWNT gels. The arrows in a−c) point out the "shoulder" in the patterns.

formation of SAXS data from the momentum transfer (Q) domain into the spatial (d) domain is given by[61−63]

$$g(d) = \frac{1}{(2\pi)^2}\int_0^\infty I(Q)Qd\sin(Qd)\exp(-DQ^2)dQ \quad (1)$$

Here, d is the inter-tubular distance, $g(d)$ is the distribution function of the inter-tubular distance, Q is the X-ray momentum transfer, $I(Q)$ is the scattering intensity (raw data presented in Supporting Information), and $\exp(-DQ^2)$ is

dx.doi.org/10.1021/am201614w | ACS Appl. Mater. Interfaces 2012, 4, 965−976

included to remove the "termination effect" of the transformation.[63,64] Generally, the parameter D is of the same order of magnitude as $1/Q^2$,[63] and its value is taken as 500 Å^2 for calculation of all the distance distribution transformations reported in this paper. The intertubular distance distribution functions, $g(d)$, for PVA/SWNT membranes prepared from SWNT gels are summarized in Figure 5. Generally, the most

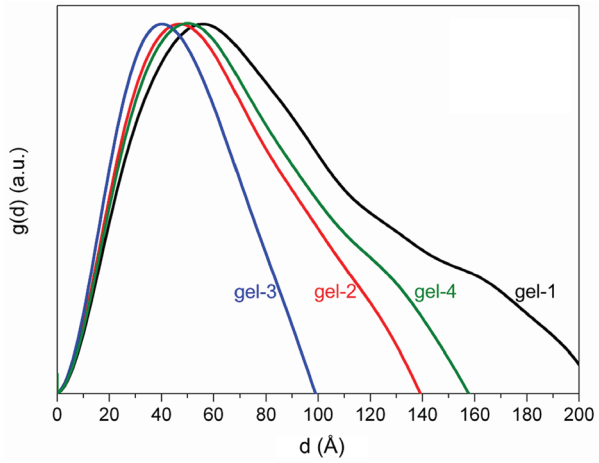

Figure 5. Inter-tubular distance distribution, derived from SAXS data, of SWNTs dispersed in PVA/SWNT composite membranes prepared from SWNT gels.

likely intertubular distance as well as the width of the distance distribution both decrease, as expected, when the SWNT volume fraction increases from 7.6% (gel-1) to 19% (gel-3). However, at higher volume fractions of 37% (gel-4), the distribution width and the most likely intertubular distance increases, perhaps due to the onset of bundle formation in the gel-4 sample as suggested by the XRD data. The most likely intertubular distance as read from Figure 5 is compared to the theoretical average intertubular distance between dispersed SWNTs at a given volume fraction in Table 1. The two

Table 1. Intertubular Distance, Outer Radius, And Length of SWNTs in PVA/SWNT Composite Membranes Prepared from SWNT Gels

	SWNT vol %			
	8	20	33	38
d from theoretical calculation (nm)	6.9	4.3	3.4	3.2
d from SAXS analysis (nm)	5.6	4.7	4.0	5.0
r_o from SAXS analysis (nm)	1.15	1.15	1.12	1.20
L from SAXS analysis (nm)	380	550	580	500

quantities are in close agreement for samples gel-1, gel-2, and gel-3. In conjunction with the XRD data, this further shows that the SWNTs in these membranes are uniformly distributed as individual nanotubes in the PVA matrix. On the other hand, the theoretical intertubular distance for the gel-4 sample is much smaller than the distance deduced from SAXS data, suggesting that the intertubular distance distribution for gel-4 is influenced by the formation of SWNT bundles instead of individually dispersed SWNTs.

Other than providing the intertubular distance information, the SAXS data can be fitted to yield information on the dimensions of SWNTs. The raw SAXS data and fits are presented in the Supporting Information, and the fitted parameters (SWNT length and outer diameter) for different samples are summarized in Table 1. The SWNT dimensions from SAXS data fitting are in excellent agreement with the range of dimensions of individual SWNTs obtained in previous reports using a variety of techniques.[49,65−68]

Mixture Separation by PVA/SWNT Composite Membranes. Recent computational studies suggest that the aluminosilicate SWNTs allow a high water diffusivity (10^{-5} to 10^{-4} cm^2/s)[44,45] that is one to two orders of magnitude higher than in other microporous materials such as zeolites,[69] and also a high adsorptive water selectivity over alcohols (greater than 50 for a 1:9 water:methanol mixture).[43,44] PVA also has high water selectivity over organics, and is the dominant polymeric material used in pervaporation membranes that dehydrate organic/water mixtures for applications such as bioethanol production.[70,71] We hypothesize that PVA/SWNT composite membranes could allow higher throughput in such applications (because of the high permeability of water in PVA) while maintaining a high selectivity over organic molecules. In this section, we investigate this hypothesis by a combination of experimental pervaporation measurements, transport modeling, and molecular simulations.

The permeation properties of PVA/SWNT composite membranes prepared from SWNT powders and SWNT gels were measured by pervaporation at 60 °C with an 80 wt % ethanol feed solution. The raw data are present in the Supporting Information and the permeability and selectivity results are summarized in Figure 6 as a function of the SWNT

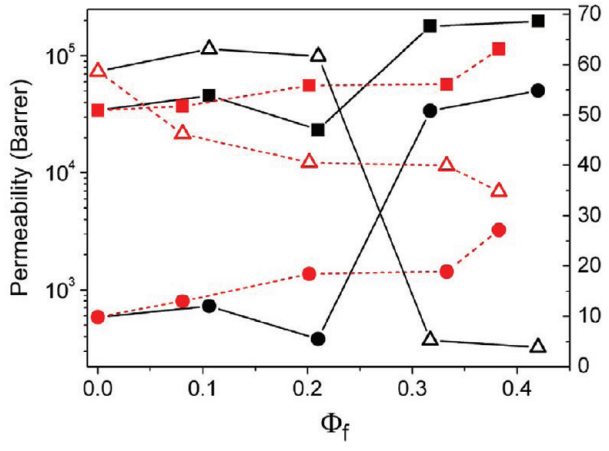

Figure 6. Water (solid squares) and ethanol (solid circles) permeability, and the water/ethanol selectivity (open triangles), of PVA/SWNT membranes prepared from SWNT powder (black solid lines) and SWNT gel (red dashed lines) with different SWNT volume fractions.

volume fraction (Φ_f), and the raw pervaporation data are presented in the Supporting Information. Membranes prepared from SWNT gels show a monotonic water permeability increase with SWNT volume fraction. The water permeability of membranes prepared with SWNT powders show no significant improvement at lower volume fractions, but the permeabilities increase abruptly after Φ_f = 0.2. Similar trends are found for the ethanol permeability. The intrinsic membrane selectivity ($S_{water/ethanol}$) is defined as the ratio of the water and ethanol permeabilities, and the values are shown in Figure 6. Membranes prepared from SWNT gels show a monotonic

decrease in selectivity from 58 (pure PVA) to 35 (Φ_f = 0.4). Membranes prepared from SWNT powders show no change in selectivity at low SWNT volume fractions, but the selectivity drops dramatically to below 5 at a higher volume fraction. These results indicate that the properties of membranes made from aggregated SWNT powders are likely affected by the occurrence of defects such as interfacial voids. Therefore, the following discussion focuses only on the composite membranes made from SWNT gels.

To gain more insight into the above membrane properties, we computationally estimated the expected water/ethanol separation performance of the SWNT at our operating conditions, and coupled this information with our recently developed model for estimating the permeability of composite membranes with tubular fillers. Figure 7 shows the predicted

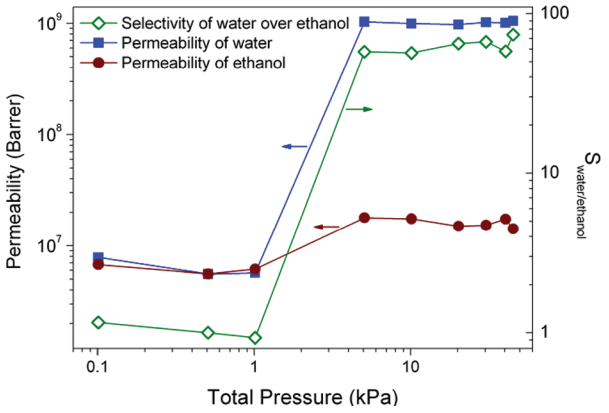

Figure 7. Predicted water and ethanol permeabilities, and water/ethanol selectivity, of the SWNT at different pressures as obtained from grand canonical Monte Carlo and molecular dynamics simulations.

permeabilities of water and ethanol, and $S_{water/ethanol}$, of the aluminosilicate SWNT in the pressure region relevant to the pervaporation measurements (0.1−45 kPa), as obtained from molecular simulations of adsorption and diffusion (as described in the Methods sections). At higher total pressures (greater than 1 kPa), the SWNT shows excellent water permeability (four orders of magnitude higher than that of PVA). At low total pressure (below 1 kPa), the SWNT has significantly diminished permeability, which is nevertheless two orders of magnitude higher than that of PVA. The ethanol permeability of the SWNT does not exhibit a strong pressure dependence, and is approximately two orders of magnitude higher than that of PVA. As a consequence, the SWNT is estimated to have a high intrinsic $S_{water/ethanol}$ of 55−75 at higher pressures, but a $S_{water/ethanol}$ of approximately unity at low pressures. Our molecular simulations provide clear mechanistic insight into this phenomenon. At low pressure, both water and ethanol transport are dominated by the strong surface interactions between these molecules and the hydroxyl groups lining the SWNT wall. Strong hydrogen bonding leads to relatively slow surface diffusion of both molecules. At higher pressures, water fills the SWNT pore to a much greater extent than ethanol, forming multilayers in the SWNT channel and exhibiting almost bulk-liquid-like diffusive behavior. The predicted high selectivity in this regime is mainly driven by strong preferential filling of water in the SWNTs and not by diffusivity differences, as shown in our previous work.[43,44]

Using the above information on the permeability of the SWNT, we interpret the experimental pervaporation results with a macroscopic transport model. The Kang−Jones−Nair (KJN) model has been derived specifically for composite membranes with tubular fillers that possess perfectly anisotropic 1D transport properties.[72] For a fixed tubular filler orientation, the KJN model predicts the effective permeability (P_{eff}) of the composite membrane as a function of the filler volume fraction (Φ_f)

$$\frac{P_{eff}}{P_m} = \left(\left(1 - \frac{\cos\theta}{\cos\theta + \frac{1}{\alpha}\sin\theta}\Phi_f\right) + \frac{P_m}{P_f}\left(\frac{1}{\cos\theta + \frac{1}{\alpha}\sin\theta}\right)\Phi_f\right)^{-1} \quad (2)$$

where P_m and P_f are the permeabilities of the matrix and the filler, respectively, θ is the filler orientation with respect to the membrane transport direction, and α is the aspect ratio of the tubular filler (length divided by outer diameter). This relation extends to a composite membrane with a random distribution of filler orientations

$$\frac{P_{eff}}{P_m} = \frac{\pi}{2}\left[\int_0^{\pi/2} \frac{P_m}{P_{eff,\theta}} d\theta\right]^{-1} \quad (3)$$

where $P_{m\ eff,\theta}$ is the permeability when the filler is aligned at an orientation θ (eq 2). The KJN model somewhat underestimates the effective permeability and can be considered as a lower bound, whereas the Hamilton-Crosser (HC) model[73,74] for isotropic cylindrical fillers can be utilized as an upper bound for predicting the effective permeability of the composite membranes

$$\frac{P_{eff}}{P_m} = \frac{P_f + 5P_m - 5(P_m - P_f)\Phi_f}{P_f + 5P_m + (P_m - P_f)\Phi_f} \quad (4)$$

The model predictions are compared to experiment in Figure 8. The experimentally measured water and ethanol permeabilities

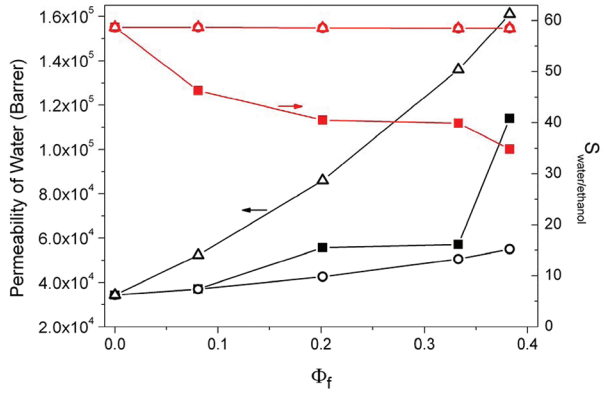

Figure 8. Comparison of water permeability and water/ethanol selectivity obtained from pervaporation experiments (solid squares), predictions of the KJN model (open circles), and predictions of the HC model (open triangles), for PVA/SWNT membranes prepared from SWNT gels.

dx.doi.org/10.1021/am201614w | ACS Appl. Mater. Interfaces 2012, 4, 965−976

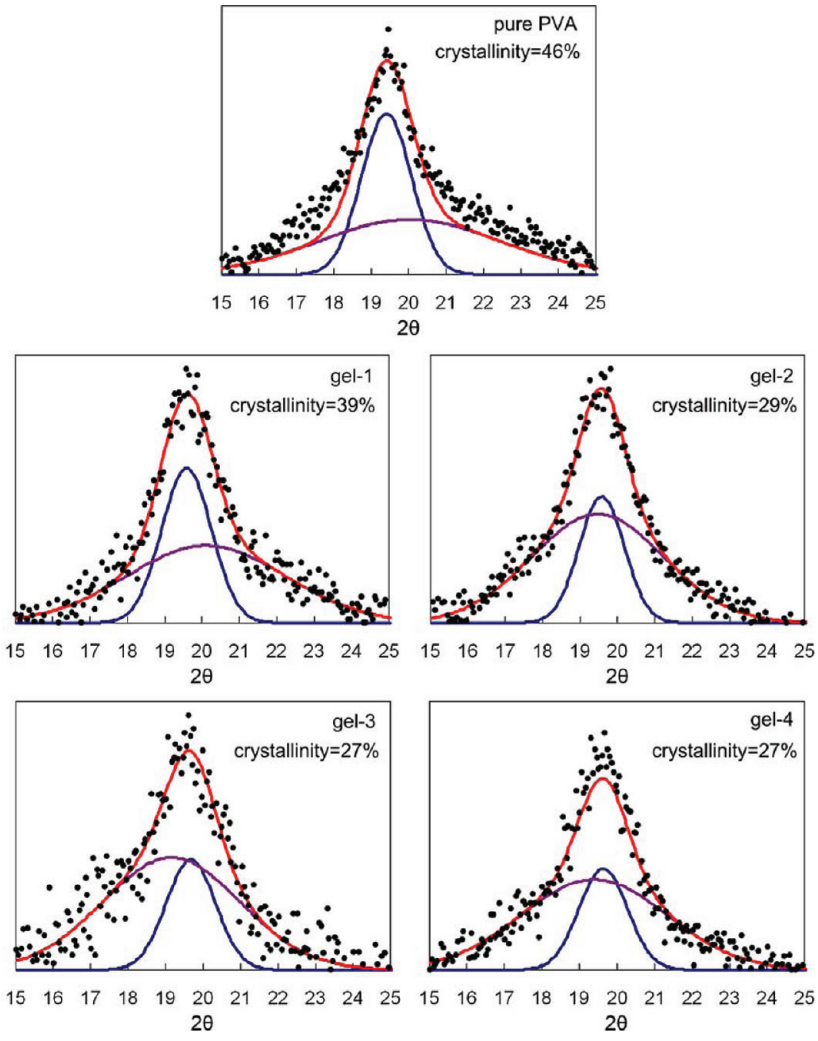

Figure 9. XRD patterns highlighting the crystalline phase in the PVA matrix, for the pure PVA and the PVA/SWNT composite membranes. The black dots are raw experimental data. Each pattern is fitted by two Gaussian distributions, representing the crystalline phase (blue) and the amorphous phase (purple), respectively. The red curves represent the summation of contributions from both the crystalline and the amorphous phases.

of PVA are used for the matrix ($P_{m,water}$ = 3.4 ×10^4 Barrer, $P_{m,ethanol}$ = 5.8 × 10^2 Barrer). The average water and ethanol permeability of the SWNTs (from Figure 8) are $P_{f,water}$ = 5×10^8 Barrer and $P_{m,ethanol}$ = 1.1 × 10^7 Barrer. The aspect ratio is α = 217 (as derived from the SAXS analysis, Table 1), and the fillers are taken to have a random orientation distribution (as known from XRD data above). Although the molecular simulations predict that the SWNT permeability varies by two orders of magnitude between low- and high-pressure conditions (Figure 7), it was found that the membrane permeation model results are insensitive to the SWNT permeability because the SWNT permeability is at least two orders of magnitude greater than the permeability of the matrix (PVA) at all pressures. It is well-known that the effective permeability of a composite membrane becomes insensitive to the filler permeability when it exceeds the matrix permeability by more than a factor of 100. The KJN model predictions of the water permeability are in good agreement with the experimental results except at Φ_f = 0.4, whereas the HC model considerably overestimates the membrane permeability.

Both the KJN and HC models predict a higher water-over-ethanol selectivity than the experimental observations. Due to the high water selectivity of both PVA (experimentally known) and the SWNT (predicted by molecular simulation), the effective membrane selectivity in both models becomes insensitive to the SWNT volume fraction. A pronounced deviation of both permeability and selectivity from the KJN model prediction is observed at higher Φ_f = 0.4 for the membranes prepared from SWNT gels. On the other hand, the membranes pwd-1 and pwd-2 prepared from SWNT powders maintain the water permeability and water/ethanol selectivity at the expected level (similar to the pure PVA membrane). These observations can be explained by several potential mechanisms, of which two appear to be most likely. Firstly, it is possible that the lower experimental value of the selectivity reflects an inaccuracy in the predictions of water selectivity in the SWNT. The permeability of ethanol during binary permeation along with water through the SWNT could be substantially different from the single-component permeability. A second possibility is the occurrence of changes in the microstructure and transport properties of the PVA matrix in the presence of large quantities of SWNT fillers and a large interfacial area between the PVA matrix and the outer surfaces of the SWNTs. For example, the molecular-scale structure of the PVA chains and the swelling

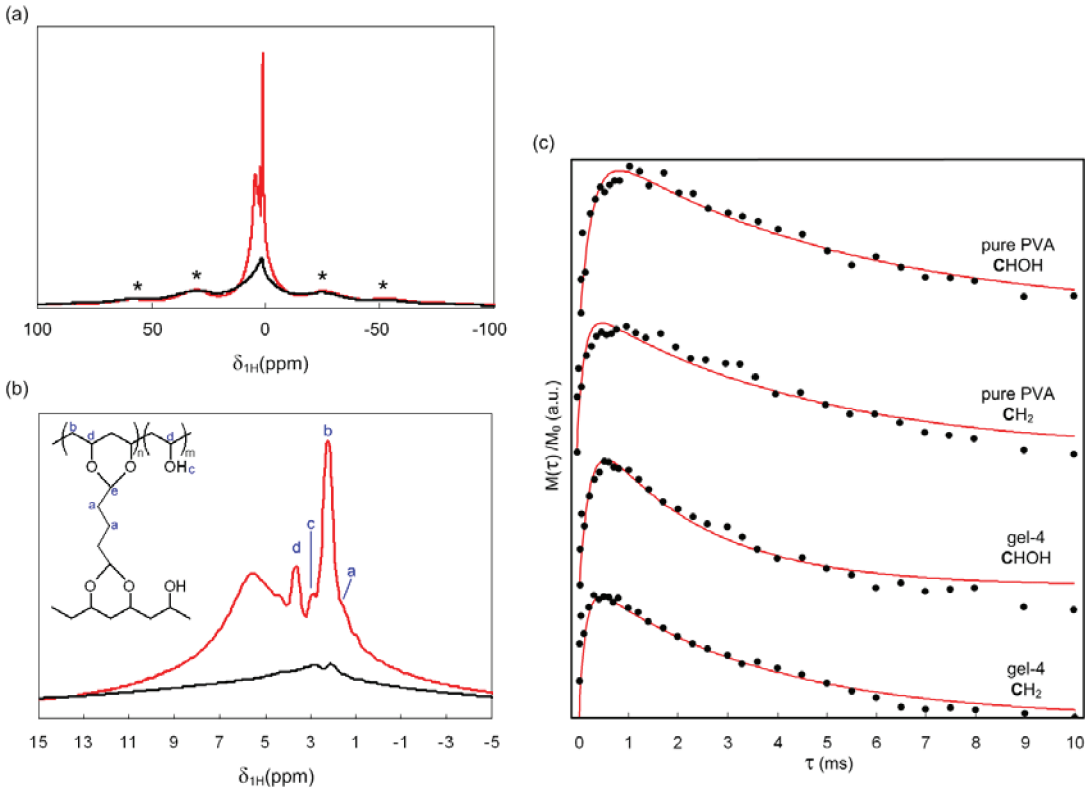

Figure 10. (a) Large spectral region of the ^{1}H spectra for the pure PVA (black) and the gel-4 (red) samples. The asterisks (*) denote to the spinning side bands. (b) A narrower spectral region of the ^{1}H spectra for the pure PVA (black) and the gel-4 (red) sample. (c) Normalized peak intensity of two different carbons (**C**HOH and **C**H_2) in PVA versus the contact time for both the pure PVA and the gel-4 samples. The black dots are the raw data and the red curves are the fitted results.

behavior of PVA in the presence of water[70,75] could be significantly altered by the presence of well-dispersed SWNT fillers. In the membranes made from SWNT gels, the average intertubular distance is in the range of 3.5−6 nm, so that there is nanoscale confinement of PVA in the spaces between the dispersed SWNTs. Furthermore, the nanotube-PVA interfacial area in these composites is relatively large ($0.32-1.5\times10^{11}$ m^2/m^3 membrane volume). As a consequence, the water permeability and selectivity of the PVA matrix in the nanocomposite membranes could deviate substantially from those of the pure PVA membranes, because of altered molecular transport properties in the nanoconfined PVA chains and near the PVA/SWNT interfaces, The PVA/SWNT membranes prepared from SWNT powder samples display poor dispersion of the SWNTs in PVA and a much lower nanotube−PVA interfacial area than the PVA/SWNT membranes prepared from SWNT gel samples, and hence the polymeric matrix remains as a continuous phase with properties essentially identical to the pure PVA membrane. The pwd-1 and pwd-2 membranes therefore have fairly similar water/ethanol transport properties as the pure PVA membrane, because the microstructure of PVA does not change significantly and the incorporated SWNTs become "inactive fillers" due to their severe agglomeration. A detailed molecular-level study of the microstructure and dynamics of the nanoconfined PVA matrix is presented in the following section.

Crystallinity and Dynamics of PVA. The crystallinity of the PVA matrix with different SWNT loadings is determined from the XRD patterns shown in Figure 9. The peak at 19.5° 2θ is assigned to the $(10\bar{1})$ reflection.[76,77] This peak can be deconvoluted into two parts: a sharp crystalline domain and a broader amorphous component. The crystallinity of the PVA matrix is taken as the ratio of the diffraction intensity of the crystalline domain to the total intensity. For composite membranes prepared using the SWNT gels, the crystallinity monotonically decreases as the SWNT loading increases (from 46% for the pure PVA membrane to 27% for the composite incorporated with 38 vol% of SWNTs). The cause of the decrease in crystallinity is perhaps that the well-dispersed SWNTs interfere with the formation of hydrogen bonds between PVA polymer chains, impeding the formation of crystalline domains in the PVA matrix.

Although XRD investigates the crystallinity of the PVA matrix, solid-state NMR is an excellent tool for studying the polymer chain dynamics. Specifically, a higher relative intensity between the central band and the spinning side band in ^{1}H NMR implies a higher proton concentration and mobility.[78−80] Given approximately the same amounts of sample packed into the NMR rotor, the PVA/SWNT composite samples would possess a lower proton concentration from PVA than the pure PVA membrane. However, a much stronger central-band-to-spinning-side-band ratio is observed for the gel-4 sample in comparison to the pure PVA membrane (Figure 10a). This observation suggests that the protons from the PVA polymer chains in the gel-4 sample have significantly higher mobility than in the pure PVA sample. Faster proton dynamics implies a higher PVA chain mobility in the matrix phase of the gel-4 sample. Furthermore, the spectral resolution for the gel-4 sample is much higher than the pure PVA sample at very similar experimental conditions (Figure 10b). Peak assignments for the area of 0-5 ppm are based upon a structure of the partially crosslinked PVA by glutaraldehyde.[81] Peaks between 5

and 10 ppm in the spectrum for the gel-4 sample are contributed by protons from SWNTs.[41,66] The proton denoted by "e" at 9−10 ppm in the partially crosslinked PVA structure, is not observed in the PVA/SWNT composite membrane, likely because of its low intensity in comparison to signals from the SWNTs in that region. Because the spectral resolution of ^{1}H NMR can be enhanced by the proton mobility,[78,79] the higher resolution seen in the gel-4 sample also supports its higher proton/PVA chain mobility in comparison to the pure PVA membrane. The observed higher PVA chain mobility for the PVA/SWNT composite membranes is in agreement with its lower crystallinity (determined by XRD), because amorphous polymer chains are expected to have faster dynamics than ordered crystalline polymers.

Additionally, ^{1}H→^{13}C cross-polarization (CP) measurements with a series of CP contact times (τ) were used to obtain microstructural and dynamical information on the PVA matrix. ^{13}C CP-NMR spectra were recorded for the pure PVA and the gel-4 sample with various contact times. In the obtained spectra, there are two distinct peaks contributed by two different carbon atoms in PVA (**C**H$_2$ and **C**HOH). The representative ^{13}C CP spectra for the pure PVA and the gel-4 membranes are presented in the Supporting Information. The peak at 45 ppm comes from **C**H$_2$ and the three adjacent peaks spanning from 60 to 80 ppm are contributed by **C**HOH with three different tacticities (from downfield to upfield: *mm*, *mr*, and *rr*). The intensity of the NMR signals for these two carbons is estimated respectively from the obtained spectra as a function of τ. The peak intensity from the raw ^{13}C CP spectra, normalized by the maximum intensity among the series of measurements, is summarized in Figure 11. Two time constants, $T_{1\rho}(^1\mathrm{H})$ and T_{CH}, can be derived by fitting the normalized peak intensity with the following equation[82,83]

$$\frac{M(\tau)}{M_0} = \left[\frac{e^{-\tau/T_{1\rho}(^1H)} - e^{-\tau/T_{\mathrm{CH}}}}{1 - T_{\mathrm{CH}}/T_{1\rho}(^1H)}\right] \quad (5)$$

where $M(\tau)$ is the intensity for a specific carbon in the ^{13}C spectra at a given contact time and M_0 is the maximum peak intensity among the performed experimental series. The derived $T_{1\rho}(^1\mathrm{H})$ and T_{CH} are summarized in Table 2.

Table 2. Parameters Derived from Contact Time Measurements on Pure PVA and gel-4 Samples

	$T_{1\rho}(^1\mathrm{H})$ (ms)		T_{CH} (ms)	
	CHOH	CH$_2$	CHOH	CH$_2$
pure PVA membrane	4.98	4.48	0.25	0.14
gel-4	2.25	1.96	0.20	0.13

For semi-crystalline materials (such as the prepared PVA/SWNT membranes), the amorphous phase acts as a relaxation sink. The constant $T_{1\rho}(^1\mathrm{H})$ for semi-crystalline materials represents the spin-diffusion time for the nuclear magnetization from the crystalline phase to the amorphous phase. The crystalline domain size, $\langle x\rangle$, can be correlated to $T_{1\rho}(^1\mathrm{H})$ as $\langle x\rangle \sim (D_s T_{1\rho}(^1\mathrm{H}))^{1/2}$, where D_s is the spin-diffusion coefficient.[83,84] The lower $T_{1\rho}(^1\mathrm{H})$ values of **C**H$_2$ and **C**HOH for the gel-4 sample in comparison to the pure PVA membrane, suggest that the SWNT-containing PVA matrix has a smaller crystalline domain size than pure PVA. On the other hand, the constant of T_{CH} represents the characteristic time for polarization transfer from the protons to the carbon nuclei.[82,85] The value of T_{CH} is thus determined by both dynamical and structural effects: the mobility of the carbon adjacent to protons, and the proton concentration around the carbon. Specifically, a short T_{CH} implies low carbon mobility or fewer protons in its immediate environment.[83,86] However, similar T_{CH} values are observed for the pure PVA and the gel-4 sample. Because our investigation suggests a higher polymer chain mobility for the gel-4 sample, the observation of similar T_{CH} values is attributed to the fact that the carbons in the PVA/SWNT composite membranes have a larger number of adjacent protons, because of the presence of SWNTs with a dense coverage of hydroxyl groups on their outer surfaces.

CONCLUSION

We have demonstrated the fabrication and detailed characterization of nanocomposite membranes containing a high loading (up to ∼40 vol %) of aluminosilicate single-walled nanotubes (SWNTs) well-dispersed in a PVA matrix. PVA/SWNT membranes prepared using SWNT gels were characterized by XRD (including rocking curve measurements), EDS, and SAXS measurements and analysis. These membranes show high uniformity, excellent dispersion of individual SWNTs (up to ∼30 vol %), and the onset of bundle formation (3-4 SWNTs per bundle) at a SWNT loading of ∼40 vol %. Analysis of SAXS data reveals the SWNT dimensions and the intertubular distance distribution. The transport properties of the PVA/SWNT membranes relevant to applications in the dehydration of ethanol/water mixtures, were investigated by pervaporation measurements, molecular simulation, and transport modeling. The membranes substantially enhance the water throughput with increasing SWNT volume fraction (up to 200% higher water permeability than pure PVA membranes at a SWNT loading of ∼40 vol %), but led to a moderate reduction of the water/ethanol selectivity from 58 (pure PVA) to 35 (SWNT loading ∼40 vol %). Detailed XRD and solid-state NMR studies suggest that the reduction of water/ethanol selectivity is likely due to the microstructural change of the PVA matrix with incorporation of SWNTs. Specifically, the crystallinity of the PVA matrix goes down (from 46 to 27% with 38 vol % SWNT incorporated) and the mobility of PVA chains increases with the presence of SWNTs in the matrix. This study shows that it is possible to fabricate SWNT/polymer nanocomposite membranes with a high-quality microstructure by inexpensive solution processing techniques, and gain insight into their permeation properties by a combination of experimental measurements and predictions by computational and theoretical methods.

ASSOCIATED CONTENT

Supporting Information

Detailed estimates of SWNT volume fraction in the PVA/SWNT membranes, SEM and TEM images, EDS elemental analysis, rocking curve XRD analysis, and ^{13}C CP/MAS NMR spectra. This material is available free of charge via the Internet at http://pubs.acs.org.

AUTHOR INFORMATION

Corresponding Author

*E-mail: sankar.nair@chbe.gatech.edu (S.N.); cjones@chbe.gatech.edu (C.W.J.).

Notes

The authors declare no competing financial interest.

■ ACKNOWLEDGMENTS

This work was supported by ConocoPhillips Company. The authors acknowledge Prof. D. G. Bucknall and Dr. J.-I. Hong (Georgia Tech) for assistance with SAXS measurements and rocking curve XRD measurements respectively, and Dr. K. C. McCarley (ConocoPhillips) for useful discussions.

■ REFERENCES

(1) Iijima, S. *Nature* **1991**, *354*, 56−58.
(2) Ismail, A. F.; Goh, P. S.; Sanip, S. M.; Aziz, M. *Sep. Purif. Technol.* **2009**, *70*, 12−26.
(3) Wang, J.; Chen, Y.; Blau, W. J. *J. Mater. Chem.* **2009**, *19*, 7425−7443.
(4) Zhang, H.; Cao, G. P.; Yang, Y. S. *Energy Environ. Sci.* **2009**, *2*, 932−943.
(5) Dai, H. J.; Javey, A.; Pop, E.; Mann, D.; Kim, W.; Lu, Y. R. *NANO* **2006**, *1*, 1−13.
(6) Bokobza, L. *Polymer* **2007**, *48*, 4907−4920.
(7) Bose, S.; Khare, R. A.; Moldenaers, P. *Polymer* **2010**, *51*, 975−993.
(8) Li, C.; Thostenson, E. T.; Chou, T. W. *Compos. Sci. Technol.* **2008**, *68*, 1227−1249.
(9) Eletskii, A. V. *Phys. Uspek.* **2009**, *52*, 209−224.
(10) Chu, K.; Wu, Q.; Jia, C.; Liang, X.; Nie, J.; Tian, W.; Gai, G.; Guo, H. *Compos. Sci. Technol.* **2010**, *70*, 298−304.
(11) Sholl, D. S.; Johnson, J. K. *Science* **2006**, *312*, 1003−1004.
(12) Whitby, M.; Quirke, N. *Nat. Nanotechnol.* **2007**, *2*, 87−94.
(13) Coleman, J. N.; Khan, U.; Blau, W. J.; Gun'ko, Y. K. *Carbon* **2006**, *44*, 1624−1652.
(14) Das, S. K.; Choi, S. U. S.; Patel, H. E. *Heat Transfer Eng.* **2006**, *27*, 3−19.
(15) Peng, F. B.; Hu, C. L.; Jiang, Z. Y. *J. Membr. Sci.* **2007**, *297*, 236−242.
(16) Majumder, M.; Chopra, N.; Andrews, R.; Hinds, B. J. *Nature* **2005**, *438*, 930−930.
(17) Majumder, M.; Chopra, N.; Hinds, B. J. *ACS Nano* **2011**, *5*, 3867−3877.
(18) Vaisman, L.; Wagner, H. D.; Marom, G. *Adv. Colloid Interface Sci.* **2006**, *128*, 37−46.
(19) Zhao, Y.-L.; Stoddart, J. F. *Acc. Chem. Res.* **2009**, *42*, 1161−1171.
(20) Lin, T.; Bajpai, V.; Ji, T.; Dai, L. M. *Aust. J. Chem.* **2003**, *56*, 635−651.
(21) Hirsch, A.; Vostrowsky, O. *Funct. Mol. Nanostruct.* **2005**, *245*, 193−237.
(22) Moniruzzaman, M.; Winey, K. I. *Macromolecules* **2006**, *39*, 5194−5205.
(23) Yamamoto, K.; Otsuka, H.; Wada, S. I.; Sohn, D.; Takahara, A. *Soft Matter* **2005**, *1*, 372−377.
(24) Grossiord, N.; Loos, J.; Regev, O.; Koning, C. E. *Chem. Mater.* **2006**, *18*, 1089−1099.
(25) Yamamoto, K.; Otsuka, H.; Takahara, A. *Polym. J.* **2007**, *39*, 1−15.
(26) Yang, H. X.; Chen, Y.; Su, Z. H. *Chem. Mater.* **2007**, *19*, 3087−3089.
(27) Jain, R.; Minus, M. L.; Chae, H. G.; Kumar, S. *Macromol. Mater. Eng.* **2010**, *295*, 742−749.
(28) Wang, R. K.; Park, H. O.; Chen, W. C.; Silvera-Batista, C.; Reeves, R. D.; Butler, J. E.; Ziegler, K. J. *J. Am. Chem. Soc.* **2008**, *130*, 14721−14728.
(29) Banerjee, S.; Hemraj-Benny, T.; Wong, S. S. *Adv. Mater.* **2005**, *17*, 17−29.
(30) Shvartzman-Cohen, R.; Nativ-Roth, E.; Baskaran, E.; Levi-Kalisman, Y.; Szleifer, I.; Yerushalmi-Rozen, R. *J. Am. Chem. Soc.* **2004**, *126*, 14850−14857.
(31) Moore, V. C.; Strano, M. S.; Haroz, E. H.; Hauge, R. H.; Smalley, R. E.; Schmidt, J.; Talmon, Y. *Nano Lett.* **2003**, *3*, 1379−1382.
(32) Tenne, R.; Seifert, G. *Annu. Rev. Mater. Res.* **2009**, *39*, 387−413.
(33) Rao, C. N. R.; Govindaraj, A. *Adv. Mater.* **2009**, *21*, 4208−4233.
(34) Mukherjee, S.; Kim, K.; Nair, S. *J. Am. Chem. Soc.* **2007**, *129*, 6820−6826.
(35) Mukherjee, S.; Bartlow, V. A.; Nair, S. *Chem. Mater.* **2005**, *17*, 4900−4909.
(36) McDonald, A.; Scott, B.; Villemure, G. *Microporous Mesoporous Mater.* **2009**, *120*, 263−266.
(37) Xiong, C. R.; Aliev, A. E.; Gnade, B.; Balkus, K. J. *ACS Nano* **2008**, *2*, 293−301.
(38) Farmer, V. C.; Fraser, A. R.; Tait, J. M. *J. Chem. Soc., Chem. Commun.* **1977**, 462−463.
(39) Wada, S. I.; Eto, A.; Wada, K. *J.Soil Sci.* **1979**, *30*, 347−352.
(40) Yang, H. X.; Wang, C.; Su, Z. H. *Chem. Mater.* **2008**, *20*, 4484−4488.
(41) Kang, D.-Y.; Zang, J.; Wright, E. R.; McCanna, A. L.; Jones, C. W.; Nair, S. *ACS Nano* **2010**, *4*, 4897−4907.
(42) Bonelli, B.; Bottero, I.; Ballarini, N.; Passeri, S.; Cavani, F.; Garrone, E. *J. Catal.* **2009**, *264*, 15−30.
(43) Zang, J.; Chempath, S.; Konduri, S.; Nair, S.; Sholl, D. S. *J. Phys. Chem. Lett.* **2010**, *1*, 1235−1240.
(44) Zang, J.; Konduri, S.; Nair, S.; Sholl, D. S. *ACS Nano* **2009**, *3*, 1548−1556.
(45) Konduri, S.; Tong, H. M.; Chempath, S.; Nair, S. *J. Phys. Chem. C* **2008**, *112*, 15367−15374.
(46) Kang, D. Y.; Zang, J.; Jones, C. W.; Nair, S. *J. Phys. Chem. C* **2011**, *115*, 7676−7685.
(47) Bottero, I.; Bonelli, B.; Ashbrook, S. E.; Wright, P. A.; Zhou, W.; Tagliabue, M.; Armandi, M.; Garrone, E. *Phys. Chem. Chem. Phys.* **2011**, *13*, 744−750.
(48) Konduri, S.; Mukherjee, S.; Nair, S. *ACS Nano* **2007**, *1*, 393−402.
(49) Konduri, S.; Mukherjee, S.; Nair, S. *Phys. Rev. B* **2006**, *74*, 033401.
(50) Robeson, L. M. *Curr. Opin. Solid State Mater. Sci.* **1999**, *4*, 549−552.
(51) Sandler, S. I. *Chemical, Biochemical, and Engineering Thermodynamics*, 4th ed. ed.; John Wiley & Sons: Hoboken, NJ, 2006.
(52) Gupta, A.; Chempath, S.; Sanborn, M. J.; Clark, L. A.; Snurr, R. Q. *Mol. Simul.* **2003**, *29*, 29−46.
(53) Cygan, R. T.; Liang, J. J.; Kalinichev, A. G. *J. Phys. Chem. B* **2004**, *108*, 1255−1266.
(54) Chen, B.; Potoff, J. J.; Siepmann, J. I. *J. Phys. Chem. B* **2001**, *105*, 3093−3104.
(55) Zang, J.; Chempath, S.; Konduri, S.; Nair, S.; Sholl, D. S. *J. Phys. Chem. Lett.* **2010**, *1*, 1235−1240.
(56) Konduri, S.; Tong, H. M.; Chempath, S.; Nair, S. *J. Phys. Chem. C* **2008**, *112*, 15367−15374.
(57) Sholl, D. S. *Acc. Chem. Res.* **2006**, *39*, 403−411.
(58) Cambedouzou, J.; Pichot, V.; Rols, S.; Launois, P.; Petit, P.; Klement, R.; Kataura, H.; Almairac, R. *Eur. Phys. J. B* **2004**, *42*, 31−45.
(59) Bendiab, N.; Almairac, R.; Rols, S.; Aznar, R.; Sauvajol, J. L.; Mirebeau, I. *Phys. Rev. B* **2004**, *69*, 195415.
(60) Qian, X.-F.; Yin, J.; Huang, J.-C.; Yang, Y.-F.; Guo, X.-X.; Zhu, Z.-K. *Mater. Chem. Phys.* **2001**, *68*, 95−97.
(61) Glatter, O.; Kratky, O. *Small Angle X-ray Scattering*; Academic Press: London, 1982.
(62) Glatter, O. *J. Appl. Crystallogr.* **1980**, *13*, 577−584.
(63) Morita, T.; Hatakeyama, Y.; Nishikawa, K.; Tanaka, E.; Shingai, R.; Murai, H.; Nakano, H.; Hino, K. *Chem. Phys.* **2009**, *364*, 14−18.
(64) Waser, J.; Schomaker, V. *Rev. Mod. Phys.* **1953**, *25*, 671−690.
(65) Tani, M.; Liu, C.; Huang, P. M. *Geoderma* **2004**, *118*, 209−220.
(66) Yucelen, G. I.; Choudhury, R. P.; Vyalikh, A.; Scheler, U.; Beckham, H. W.; Nair, S. *J. Am. Chem. Soc.* **2011**, *133*, 5397−5412.
(67) Vandergaast, S. J.; Wada, K.; Wada, S. I.; Kakuto, Y. *Clays Clay Miner.* **1985**, *33*, 237−243.

(68) Zhao, M. W.; Xia, Y. Y.; Mei, L. M. *J. Phys. Chem. C* **2009**, *113*, 14834−14837.
(69) Demontis, P.; Jobic, H.; Gonzalez, M. A.; Suffritti, G. B. *J. Phys. Chem. C* **2009**, *113*, 12373−12379.
(70) Chapman, P. D.; Oliveira, T.; Livingston, A. G.; Li, K. *J. Membr. Sci.* **2008**, *318*, 5−37.
(71) Van Baelen, D.; Van der Bruggen, B.; Van den Dungen, K.; Degreve, J.; Vandecasteele, C. *Chem. Eng. Sci.* **2005**, *60*, 1583−1590.
(72) Kang, D.-Y.; Jones, C. W.; Nair, N. *J. Membr. Sci.* **2011**, submitted.
(73) Skoulidas, A. I.; Ackerman, D. M.; Johnson, J. K.; Sholl, D. S. *Phys. Rev. Lett.* **2002**, *89*, 185901.
(74) Hamilton, R. L.; Crosser, O. K. *Ind. Eng. Chem. Fund.* **1962**, *1*, 187−191.
(75) Zhang, Q. G.; Liu, Q. L.; Zhu, A. M.; Xiong, Y.; Ren, L. *J. Membr. Sci.* **2009**, *335*, 68−75.
(76) Assender, H. E.; Windle, A. H. *Polymer* **1998**, *39*, 4295−4302.
(77) Ricciardi, R.; Auriemma, F.; De Rosa, C.; Laupretre, F. *Macromolecules* **2004**, *37*, 1921−1927.
(78) Eckert, H.; Yesinowski, J. P.; Silver, L. A.; Stolper, E. M. *J. Phys. Chem.* **1988**, *92*, 2055−2064.
(79) Yesinowski, J. P.; Eckert, H.; Rossman, G. R. *J Am. Chem. Soc.* **1988**, *110*, 1367−1375.
(80) Vega, A. J.; Scherer, G. W. *J. Non-Cryst. Solids* **1989**, *111*, 153−166.
(81) Kobayashi, M.; Ando, I.; Ishii, T.; Amiya, S. *Macromolecules* **1995**, *28*, 6677−6679.
(82) Voelkel, R. *Angew. Chem., Int. Ed.* **1988**, *27*, 1468−1483.
(83) Gabrielse, W.; Gaur, H. A.; Feyen, F. C.; Veeman, W. S. *Macromolecules* **1994**, *27*, 5811−5820.
(84) Bai, S.; Hu, J. Z.; Pugmire, R. J.; Grant, D. M.; Taylor, C. M. V.; Rubin, J. B.; Peterson, E. J. *Macromolecules* **1998**, *31*, 9238−9246.
(85) Ibbett, R. N. *NMR Spectroscopy of Polymers*; 1st ed.; Blackie Academic & Professional: London, 1993.
(86) Rasburn, J.; Seker, F.; Kulbaba, K.; Klein, P. G.; Manners, I.; Vancso, G. J.; Macdonald, P. M. *Macromolecules* **2001**, *34*, 2884−2891.